The Astrophysical Journal Letters, 851:L3 (5pp), 2017 December 10 https://doi.org/10.3847/2041-8213/aa9b2c

The Brightest Known H_2CO Maser in the Milky Way: G339.88-1.26

Xi Chen[1,2], Zhi-Qiang Shen[2,3], Simon P. Ellingsen[4], Xiao-Qiong Li[2,5], Kai Yang[2,5], Hong-Ying Chen[2,5], and Jian Dong[2,3]
[1] Center for Astrophysics, GuangZhou University, Guangzhou 510006, China; chenxi@gzhu.edu.cn
[2] Shanghai Astronomical Observatory, Chinese Academy of Sciences, Shanghai 200030, China; chenxi@shao.ac.cn
[3] Key Laboratory of Radio Astronomy, Chinese Academy of Sciences, Nanjing, JiangSu 210008, China
[4] School of Physical Sciences, University of Tasmania, Hobart, TAS 7001, Australia
[5] University of Chinese Academy of Sciences, 19A Yuquanlu, Beijing 100049, China
Received 2017 October 13; revised 2017 November 10; accepted 2017 November 13; published 2017 December 5

Abstract

We report the detection of the strongest $1_{01}-1_{11}$ 6 cm H_2CO emission in our Galaxy. The detection toward the massive star-forming region G339.88-1.26 was made using the Shanghai Tianma radio telescope (TMRT). The G339.88-1.26 star formation region hosts one of the strongest 6.7 GHz methanol masers and has an accompanying collimated, ionized jet seen in radio continuum free–free emission. The peak flux density of the detected H_2CO emission is ~19 Jy, one order of magnitude stronger than the nine previously known H_2CO maser sources. The corresponding luminosity is also brighter than has been observed in previous H_2CO maser sources, even those detected in the Central Molecular Zone of our Galaxy. A TMRT on-the-fly map of the region shows a point-like source structure and this, combined with the spectral characteristics of the H_2CO emission (multiple, narrow components), leads us to conclude that the detected H_2CO emission is masing (with a brightness temperature in excess of 10^4 K). The detection of a very strong H_2CO maser in G339.88-1.26 suggests that ionized jet/outflow environments might provide efficient maser pumping for this transition, with the ionized jet/outflow-driven shock causing collisional excitation, and are also able to provide additional seed photons for maser amplification of the radio continuum emission.

Key words: ISM: molecules – masers – radio lines: ISM – stars: formation

1. Introduction

A number of surveys for H_2CO masers in the $1_{01}-1_{11}$ 6 cm transition have been made toward massive young stellar objects (MYSOs; e.g., Araya et al. 2004, 2007b, 2008) and evolved stars (Araya et al. 2015). H_2CO 6 cm absorption has been studied toward hundreds of sources, but to date only nine H_2CO maser sources have been detected in our Galaxy (see Araya et al. 2007a and references therein; Araya et al. 2015; Ginsburg et al. 2015). All the detected H_2CO masers are associated with regions of massive star formation (e.g., Araya et al. 2004, 2007b, 2008, 2015) and appear to trace a very early phase of the star formation process (e.g., Araya et al. 2006). At present, the reason for the rarity of H_2CO masers in our Galaxy is not clear. It may reflect that the physical conditions required to excite the H_2CO masers are specific and short-lived (Hoffman et al. 2003; Araya et al. 2007a). If that is the case, then the excitation mechanism for H_2CO masers can be used to investigate these specific and short-lived physical conditions. However, at present, the pumping mechanism of the H_2CO masers is poorly understood.

Some models have been proposed to explain the H_2CO maser excitation (see Araya et al. 2007a). A model with radiation caused by radio continuum from a background compact H II region with emission measure greater than 10^8 pc cm^{-6} can explain the 6 cm H_2CO maser detected toward NGC 7538 (Boland & de Jong 1981). However, such background H II regions are not observed near some H_2CO maser sources (e.g., Araya et al. 2008), thus indicating that this mechanism cannot explain most of the observed masers. Hoffman et al. (2003) suggest that collisional pumping by shocks driven by an expanding H II region might explain the masers toward NGC 7538 and G29.96-0.02. Alternatively, Chen et al. (2017) proposed that the variability detected in the 6 cm H_2CO masers in NGC 7538 may be due to a high-velocity shock ($> 80\,km\,s^{-1}$), which is most likely to be driven by a jet or outflow, but unlikely to be driven by an expanding H II region. If this is the general mechanism for producing H_2CO masers, then we predict that they are likely to be present in sources associated with jets/outflows. Hence, searches for H_2CO masers associated with star formation regions where jets or outflows have been detected provide a direct test of this hypothesis.

In this Letter, we report the detection of the strongest (~19 Jy) H_2CO maser detected so far in our Galaxy. The detection is from the massive star-forming region G339.88-1.26, which is one of the strongest (1520 Jy; Caswell et al. 2011) 6.7 GHz methanol masers. This source has been well studied in a range of maser and thermal molecular transitions (e.g., Norris et al. 1993; de Buizer et al. 2002; Ellingsen et al. 2004, 2011) and in the continuum emission at radio and infrared bands (e.g., Ellingsen et al. 1996, 2005; Purser et al. 2016). The radio continuum observations of this source show a collimated, ionized jet elongated at a position angle of ~45° (Ellingsen et al. 1996; Purser et al. 2016). The distance to this source is 2.1 kpc, determined from trigonometric parallax measurements of the 6.7 GHz methanol masers using the Australian Long Baseline Array (Krishnan et al. 2015).

2. Observation

The observations of the 6 cm H_2CO $1_{01}-1_{11}$ transition toward G339.88-1.26 were undertaken with the Tianma radio telescope

(TMRT), which has a diameter of 65 m. The cryogenically cooled C-band receiver that can cover the frequency range 4–8 GHz was used in the observation. The digital backend system (DIBAS; see Li et al. 2016) was used for data recording. Two sub-bands covering the frequency ranges 4.4–5.2 GHz and 6.0–6.8 GHz were observed. Each sub-band was configured to record eight spectral windows with a bandwidth of 23.4 MHz for each, covering the important astronomical lines in these frequency ranges. In this Letter, we focus on the 1_{01}–1_{11} H_2CO and 5_1–6_0 A^+ CH_3OH lines. The adopted rest frequencies of the H_2CO and CH_3OH transitions are 4.829657 and 6.668519 GHz, respectively. Each spectral window has 16,384 channels, yielding a channel spacing of 1.431 KHz, corresponding to ∼0.089 and ∼0.064 km s^{-1} for H_2CO and CH_3OH, respectively. The system temperature for the observations was in the range 40–50 K. The beam size was ∼4′ and ∼3′ for the H_2CO and CH_3OH transitions, respectively. The adopted target position of G339.88-1.26 was $\alpha = 16^h52^m04\overset{s}{.}7$ and $\delta = -46°08'34''$ (J2000). Even though the elevation of the telescope was low (only ∼10°–12°) during the observations, thanks to the good performance of the active surface system, which corrects for the effects of gravitational deformation (Dong et al. 2016), the achieved aperture efficiency of the telescope was good to ∼60%, corresponding to a sensitivity of 1.4 Jy K^{-1}.

Single-pointing, position-switching observations were made toward G339.88-1.26 on 2017 September 22 and 23. The observations consisted of three repetitions of 2 minute ON/OFF cycles using two different off-positions, which were offset from the target position by (+0.°4, 0°) and (−0.°4, 0°) in right ascension (R.A.) and declination (decl.), respectively. The typical rms noise of the observations was ∼80 mJy per spectral channel. We found that the H_2CO emission spectrum was the same when quotient spectra were produced using either of the two different off-positions, demonstrating that there is no significant contribution to the spectrum from any background H_2CO absorptions at the off-position locations. A final spectrum was created by averaging the data from all scans and then subtracting a fitted baseline to the channels with no H_2CO emission.

Additional observations were undertaken on 2017 September 24 to determine the spatial scale of the detected H_2CO emission and absorption around G339.88-1.26. We used the on-the-fly (OTF) mapping mode to image a square region (7′ in both R.A. and decl.), centered on the target position of G339.88-1.26. The TMRT mapped the region, first with the primary scan along R.A. and a second time with the primary scan along decl. The antenna was driven at 9″ per second for the OTF mapping observations with a spacing of 9″ between adjacent scans. The overall observing time of the OTF observations was about 100 minutes. We performed all the data reduction of the spectral line observations using the GILDAS/CLASS and GILDAS/GREG packages.

3. Results

3.1. H_2CO Spectrum from Single-pointing Observations

The TMRT single-point observations were taken on two consecutive days. They have similar noise levels and, within the uncertainties, they show the same H_2CO spectrum toward G339.88-1.26. We combined the spectra from the two days to improve the signal-to-noise ratio (S/N) and Figure 1 shows the combined H_2CO spectrum, which has an rms noise of ∼60 mJy per channel. It clearly shows strong emission (with a peak flux density of ∼19 Jy) blueshifted with respect to a broad absorption feature. The H_2CO emission covers the velocity range from −39 to −34.5 km s^{-1} and appears to be a blend of multiple narrow spectral features. In contrast, the absorption feature is well fitted by a single component and covers the velocity range from −34.5 to −27 km s^{-1}. To characterize the emission and absorption features, we performed Gaussian fitting of the spectrum using multiple components. We found that five emission components and one absorption component provided the best fit to the spectrum. The Gaussian fitting parameters are listed in Table 1.

The five emission components show narrow line widths that have a range of 0.4–1.2 km s^{-1}, but the absorption is significantly broader with a line width of 3.7 km s^{-1}. This spectrum is similar to that of the known H_2CO maser sources NGC 7538, G25.83-0.18, G32.74-0.07, and IRAS 18566 +0408 (e.g., Chen et al. 2017). The typical line widths of the emission and absorption in these known H_2CO maser sources are approximately 1 km s^{-1} and a few km s^{-1}, respectively. However, the previously detected H_2CO maser sources typically only show a single maser emission feature, with the exception being NGC 7538, which has two narrow maser

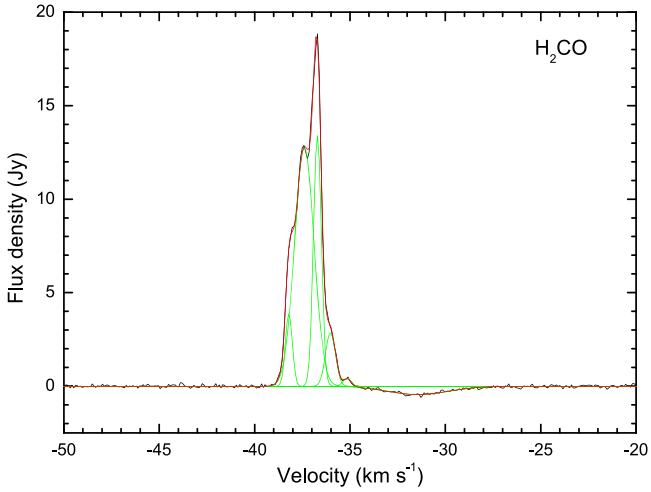

Figure 1. Spectrum of the 6 cm H_2CO emission and absorption toward G339.88-1.26 from a single-point observation with the TMRT. The green solid lines represent the individual components determined from Gaussian fitting, and the red solid line shows the sum of the Gaussian fitting components for all spectral features.

Table 1
Line Parameters of the 6 cm H_2CO Detected with the TM Telescope

v_{LSR} (km s^{-1}) (1)	Δv (km s^{-1}) (2)	S (Jy km s^{-1}) (3)	P Jy (4)
−38.21(0.01)	0.43(0.02)	1.76(0.16)	3.88
−37.40(0.01)	1.20(0.03)	16.24(0.46)	12.77
−36.71(0.01)	0.49(0.01)	6.92(0.27)	13.42
−36.02(0.01)	0.62(0.03)	1.88(0.10)	2.87
−35.15(0.04)	0.51(0.11)	0.23(0.05)	0.42
−31.44(0.10)	3.72(0.25)	−1.74(0.11)	−0.44

Note. Columns (1)–(4): the velocity at peak v_{LSR}, the FWHM line width Δv, the velocity-integrated intensity S, and the peak flux density of each spectral feature.

features. In contrast, G339.88-1.26 is composed of five narrow emission features.

The flux density of the previously known H_2CO masers ranges between a few tens of mJy and ~2 Jy (for the strongest masers in Sgr B2 and NGC 7538; Hoffman et al. 2007; Chen et al. 2017), with most masers of the order of ~100 mJy. G339.88-1.26 shows the strongest H_2CO emission known to date, with a peak flux density of ~19 Jy, one order of magnitude stronger than that in NGC 7538 and Sgr B2. The distances to G339.88-1.26 and NGC 7538 determined from very long baseline interferometry (VLBI) observations of masers are 2.10 kpc and 2.65 kpc, respectively (Moscadelli et al. 2009; Krishnan et al. 2015). So these two sources are at a similar distance, hence the luminosity of the H_2CO emission in G339.88-1.26 is also approximately one order of magnitude higher than that in NGC 7538. Compared with the H_2CO masers in the Central Molecular Zone (CMZ) of the Milky Way, associated with Sgr B2 (Hoffman et al. 2007) and Cloud C (Ginsburg et al. 2015), we find that the luminosity of the H_2CO emission in G339.88-1.26 is similar to the brightest emission (component A in Sgr B2; Hoffman et al. 2007) in the CMZ (adopting a distance of 7.8 kpc to Sgr B2; Reid et al. 2009). However, if we used the integrated luminosity, we find a luminosity of 119 Jy km s^{-1} kpc^2 for G339.88-1.26, which is higher than that in component A (~80 Jy km s^{-1} kpc^2) of Sgr B2.

3.2. H_2CO Image from OTF Observations

We spatially re-sampled the TMRT OTF data using a cell size of 10″ to construct an image of the H_2CO emission and absorption in G339.88-1.26. For the emission, the image includes the velocity-integrated intensity over the range −39 to −34.5 km s^{-1}. For the absorption, the image was constructed from the velocity-integrated intensity over the range −34.5 to −27 km s^{-1}. Figure 2 shows the integrated intensity maps of the H_2CO emission and absorption, overlaid on a three-color image constructed from the 3.4, 4.6, and 12.0 μm band data (coded as blue, green, and red, respectively) from the *Wide-field Infrared Survey Explorer* (*WISE*). The OTF map shows that the H_2CO emission is point-like at the resolution of the TMRT (it has the same scale as the telescope beam), while the absorption shows an extended structure (larger than the beam size). The peak position of the integrated emission is centered on the target position of the single-pointing observations (i.e., the location of other maser species detected toward G339.88-1.26). The good spatial correspondence demonstrates that G339.88-1.26 is the driving source for the H_2CO emission. In contrast, the integrated absorption peaks at the location of a *WISE* point source with enhanced 4.6 μm emission, offset to the southwest of the emission in G339.88-1.26 with an angular separation of ~100″. The absorption is mainly confined to the region west of the G339.88-1.26 H_2CO emission.

3.3. Comparison of the H_2CO and CH_3OH Spectra

Comparing the H_2CO emission with the 6.7 GHz CH_3OH maser spectrum simultaneously observed by the TMRT, we find that at least three of the five H_2CO emission features are very closely aligned in velocity with CH_3OH maser components. Figure 3 shows a comparison of the H_2CO and CH_3OH spectra in G339.88-1.26 and the close correspondence of the H_2CO components at −38.2, −37.4, and −36.7 km s^{-1} with CH_3OH maser features. Similar close correspondence in velocity between

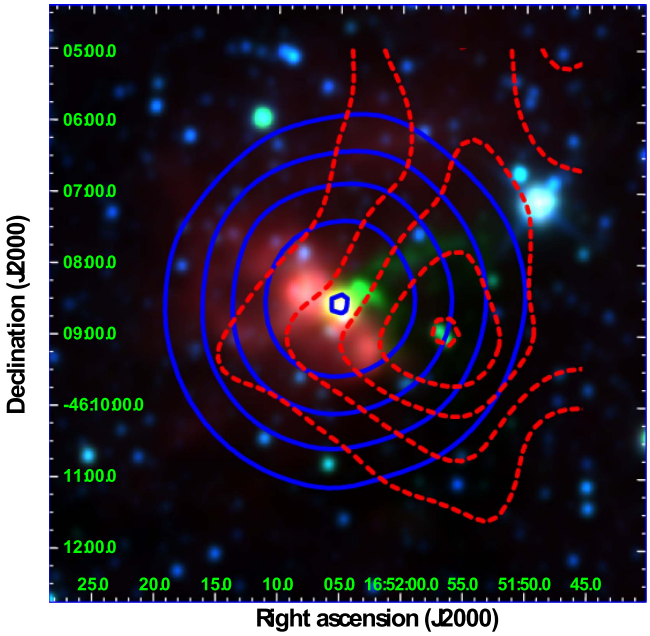

Figure 2. Velocity-integrated emission and absorption image of the 6 cm H_2CO transition near G339.88-1.26 obtained from the TMRT OTF observations. The background is the color-synthesized image from the *WISE* 3.4 μm (blue), 4.6 μm (green), and 12.0 μm (red) bands. The solid blue and dashed red contours represent the velocity-integrated emission in a velocity range of (−39, −34.5) km s^{-1} and absorption in a velocity range of (−34.5, −27) km s^{-1}, respectively. The contour levels are 6–22 Jy km s^{-1} in steps of 4 Jy km s^{-1} for the emission also reflecting the size of the beam, and −0.9–2.9 Jy km s^{-1} in steps of −0.5 Jy km s^{-1} for the absorption.

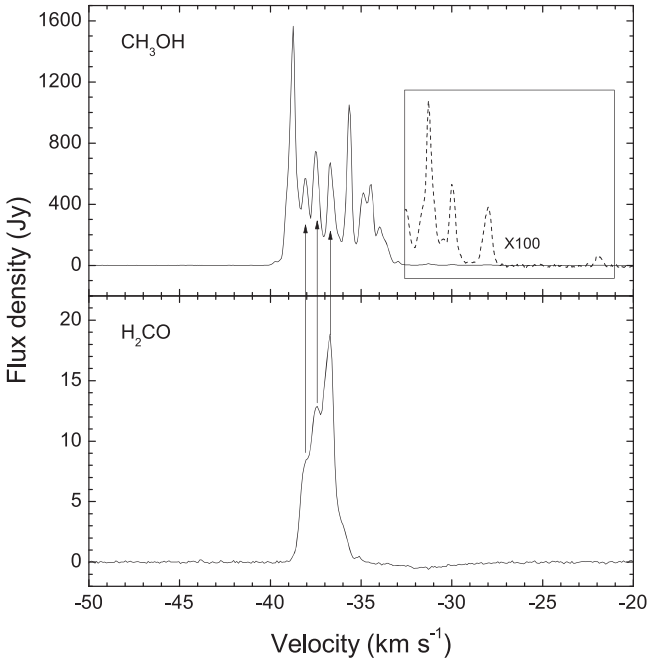

Figure 3. Comparison of the H_2CO and CH_3OH maser spectra toward the target position of G339.88-1.26. The corresponding spectral features are connected between H_2CO and CH_3OH by lines with upward arrows.

H_2CO and CH_3OH masers has been noted in some other H_2CO maser sources, e.g., G0.38+0.04 (Ginsburg et al. 2015). Interestingly, the two strongest methanol maser features are at velocities of −38.8 and −35.6 km s^{-1}, where no H_2CO emission features are detected. Indeed, the two strongest methanol maser

features appear to bracket the H_2CO emission range. The similarity in velocities suggests that the three H_2CO and CH_3OH features may be spatially coincident. However, further higher angular resolution observations are required to obtain the distributions of both the H_2CO and CH_3OH masers to determine if this is the case.

4. Discussions

4.1. Thermal Emission or Maser Feature?

Figure 1 shows that the 6 cm H_2CO emission in G339.88-1.26 is composed of five narrow components. This differs from the H_2CO emission detected in Orion KL, which is the only currently known source where 6 cm H_2CO emission appears to be thermally excited (Zuckerman et al. 1975; Mangum et al. 1993). No H_2CO maser emission has been detected toward Orion KL; thermal emission with a peak $T_B \sim 40$ K was detected there (Mangum et al. 1993). The thermal emission from Orion KL has a spectral profile consisting of a single, wide Gaussian profile with a line width of $\sim$3 km s^{-1} (Zuckerman et al. 1975). Moreover the narrow line width of the H_2CO emission in G339.88-1.26 is similar to that found in other known maser sources.

If we assume that all the detected H_2CO emission originates from a region with angular size less than 10″ (corresponding to the cell size of the TMRT OTF image; see Section 3.2), then the implied brightness temperature of the peak H_2CO emission is greater than $\sim$14,400 K. On the other hand, the H_2CO masers are usually located close to the 6.7 GHz CH_3OH masers (see Araya et al. 2010), in G339.88-1.26 the CH_3OH masers are distributed over a region of 1.″5 (see Section 4.2), and if we assume that the H_2CO emission covers a similar angular scale, then we infer a brightness temperature of 5×10^5 K. Either of these brightness temperature estimates strongly suggest that the detected emission is unlikely to be thermal in nature. Combining all these properties, we conclude that the detected H_2CO emission from G339.88-1.26 is masing.

4.2. What Are the Extreme Conditions in G339.88-1.26?

A natural question raised by the current observations is whether there are extreme physical, chemical, or kinematic conditions in this source responsible for producing such strong masers compared to other star-forming regions with H_2CO maser emission. G339.88-1.26 is located in a cluster environment with multiple high-mass protostellar objects. High-resolution images made with the mid-infrared imager/spectrometer OSCIR at the Keck Observatory have resolved the mid-infrared emission into three sources (1A, 1B, and 1C) that all lie within a region of 1.″5 (de Buizer et al. 2002). Interferometric radio observations have revealed an elongated, ionized jet/outflow at a position angle of $\sim$45° with a scale of 15″, approximately perpendicular to the distribution of the 6.7 GHz methanol maser spots (Ellingsen et al. 1996; Purser et al. 2016). de Buizer et al. (2002) identified MIR source 1B as the driving source for the ionized jet/outflow, although the registration between the radio and MIR was somewhat uncertain. On larger scales, the three-color *WISE* image shows an extended 12 μm emission lobe (see Figure 2, the 12 μm emission is red in this image). The orientation of the large-scale infrared emission is the same as that of the ionized jet/outflow and may represent an ionized region produced by the UV emission from a star or cluster. Moreover, significant extended 4.6 μm emission (colored "green" in Figure 2) is present in the three-color *WISE* image. In general, extended emission seen predominantly in the 4.6 μm band is indicative of the presence of shock-excited molecular H_2 and CO, produced in an outflow from an MYSO (e.g., Cyganowski et al. 2008; Chen et al. 2013). The *WISE* data suggest that MIR source 1C is more likely the driving source for such an outflow because the source shows similar extended structure in a small scale (a few arcseconds) in the MIR band (18 μm; see de Buizer et al. 2002) to the *WISE* data.

VLBI observations have shown that methanol masers are actually distributed in two groups, distributed over a region with an angular scale of 1.″5, and oriented southeast to northwest (e.g., de Buizer et al. 2002; Dodson 2008). de Buizer et al. (2002) suggest that the alignment of the two groups of methanol masers is to the regions around the MIR sources 1B and 1C. The methanol maser components with velocities < -36 km s^{-1} are mainly located in the southeastern region (i.e., source 1B), whereas those with velocities > -36 km s^{-1} are mainly in the northwestern region (source 1C). The H_2CO maser components primarily have line-of-sight velocities < -36 km s^{-1}, and three of the H_2CO maser features have velocities that align the with methanol masers (see Section 3.3). If these H_2CO masers are also spatially coincident with the methanol masers, then the H_2CO masers are associated with MIR source 1B. This assumption is supported by the observational evidence that the spatial distributions for the H_2CO and CH_3OH maser components with similar velocities were found to be spatially coincident within 0.″1 in IRAS 18566+0408 (Araya et al. 2010). Therefore, this suggests that the H_2CO masers might be favored in sources with ionized jets/outflows. The H_2CO maser variability detected in NGC 7538 supports the hypothesis that they could be excited by collisions via a jet/outflow-driven shock (Chen et al. 2017). The much stronger maser emission detected in G339.88-1.26 suggests that an ionized jet/outflow-driven shock might provide better conditions for the maser pumping. Moreover, the background radio continuum free–free emission from the ionized jet/outflow region could provide additional seed photons for maser amplification. Further searches for H_2CO masers toward sources with ionized jets/outflows (e.g., the sample compiled by Purser et al. 2016) could be made to test whether or not such mechanisms play an important role in H_2CO maser excitation.

5. Summary

We have detected the so far strongest H_2CO maser in the Galaxy toward the massive star-forming region G339.88-1.26 using the Shanghai Tianma Radio telescope. The maser emission from the 6 cm H_2CO transition has a peak flux density of $\sim$19 Jy, one order of magnitude greater than previously known maser H_2CO sources in our Galaxy. This detection increases the number of known Galactic H_2CO maser sources to 10. The detection from the 6 cm H_2CO transition shows both emission and absorption, with multiple narrow spectral features ($\sim$1 km s^{-1}) seen in the emission. The H_2CO emission is compact at the resolution of the current observations, and depending upon the assumptions made we can place a lower limit on the brightness temperature of the H_2CO masers of at least 14,400 K, and likely $\sim 5 \times 10^5$ K. The combination of the spectral properties and high brightness temperature of the H_2CO emission leads us to conclude that it is a maser. Based on the assumption that the H_2CO and CH_3OH maser features

with the same line-of-sight velocities are spatially coincident, we further suggest that the H_2CO maser is associated with the driving source of the collimated, ionized jet in G339.88-1.26. This suggests that collisional excitation via an ionized jet/outflow-driven shock may play an important role in the production of stronger H_2CO masers.

We thank an anonymous referee for helpful comments that improved the manuscript. We thank the assistance of the TMRT operators during the observations. This work was supported by the National Natural Science Foundation of China (11590781); the Strategic Priority Research Program of the Chinese Academy of Sciences (CAS; grant No. XDA04060701), Key Laboratory for Radio Astronomy, CAS; Guangdong innovation Group for Astrophysics (2014KCXTD014), and support for Key Subjects (Astrophysics) of Guangdong Province and Guangzhou City.

ORCID iDs

Xi Chen https://orcid.org/0000-0002-5435-925X
Simon P. Ellingsen https://orcid.org/0000-0002-1363-5457

References

Araya, E., Hofner, P., Goss, W. M., et al. 2006, ApJL, 643, L33
Araya, E., Hofner, P., & Goss, W. M. 2007a, in IAU Symp. 242, Astrophysical Masers and their Environments, ed. J. Chapman & W. A. Baan (Cambridge: Cambridge Univ. Press), 110
Araya, E., Hofner, P., Goss, W. M., et al. 2007b, ApJS, 170, 152
Araya, E., Hofner, P., Goss, W. M., et al. 2010, ApJL, 717, L133
Araya, E., Hofner, P., Linz, H., et al. 2004, ApJS, 154, 579
Araya, E. D., Hofner, P., Goss, W. M., et al. 2008, ApJS, 178, 330
Araya, E. D., Olmi, L., Ortiz, J. M., et al. 2015, ApJS, 221, 10
Boland, W., & de Jong, T. 1981, A&A, 98, 149
Caswell, J. L., Fuller, G. A., Green, J. A., et al. 2011, MNRAS, 417, 1964
Chen, X., Gan, C.-G., Ellingsen, S. P., et al. 2013, ApJS, 206, 9
Chen, X., Shen, Z.-Q., Li, X.-Q., et al. 2017, MNRAS, 466, 4364
Cyganowski, C. J., Whitney, B. A., Holden, E., et al. 2008, AJ, 136, 2391
de Buizer, J. M., Walsh, A. J., Piña, R. K., Phillips, C. J., & Telesco, C. M. 2002, ApJ, 564, 327
Dodson, R. 2008, A&A, 480, 767
Dong, J., Jin, H.-L., Ye, Q., et al. 2016, Proc. SPIE, 9913, 991306
Ellingsen, S. P., Breen, S. L., Sobolev, A. M., et al. 2011, ApJ, 742, 109
Ellingsen, S. P., Cragg, D. M., Lovell, J. E. J., et al. 2004, MNRAS, 354, 401
Ellingsen, S. P., Norris, R. P., & McCulloch, P. M. 1996, MNRAS, 279, 101
Ellingsen, S. P., Shabala, S. S., & Kurtz, S. E. 2005, MNRAS, 357, 1003
Ginsburg, A., Walsh, A., Henkel, C., et al. 2015, A&A, 584, L7
Hoffman, I. M., Goss, W. M., & Palmer, P. 2007, ApJ, 654, 971
Hoffman, I. M., Goss, W. M., Palmer, P., & Richards, A. M. S. 2003, ApJ, 598, 1061
Krishnan, V., Ellingsen, S. P., Reid, M. J., et al. 2015, ApJ, 805, 129
Li, J., Shen, Z.-Q., Wang, J.-Z., et al. 2016, ApJ, 824, 136
Mangum, J. G., Wootten, A., & Plambeck, R. L. 1993, ApJ, 409, 282
Moscadelli, L., Reid, M. J., Menten, K. M., et al. 2009, ApJ, 693, 406
Norris, R. P., Whiteoak, J. B., Caswell, J. L., Wieringa, M. H., & Gough, R. G. 1993, ApJ, 412, 222
Purser, S. J. D., Lumsden, S. L., Hoare, M. G., et al. 2016, MNRAS, 460, 1039
Reid, M. J., Menten, K. M., Zheng, X. W., Brunthaler, A., & Xu, Y. 2009, ApJ, 705, 1548
Zuckerman, B., Rickard, L. J., & Palmer, P. 1975, ApJ, 197, 571